RESEARCH Open Access



CircTTC13 promotes sorafenib resistance in hepatocellular carcinoma through the inhibition of ferroptosis by targeting the miR-513a-5p/SLC7A11 axis

Ying Zhang^{1,2†}, Ruiwei Yao^{4,5†}, Mingyi Li^{6†}, Chongkai Fang^{7†}, Kunliang Feng⁸, Xiuru Chen⁷, Jinan Wang^{1,5}, Rui Luo^{4,5}, Hangian Shi^{4,5}, Xingiu Chen^{4,5}, Xilin Zhao^{1,3}, Hanlin Huang^{4,5}, Shuwei Liu^{4,5}, Bing Yin^{4,5} and Chong Zhong^{1,3,5*}

Abstract

The high mortality rate from hepatocellular carcinoma (HCC) is due primarily to challenges in early diagnosis and the development of drug resistance in advanced stages. Many first-line chemotherapeutic drugs induce ferroptosis, a form of programmed cell death dependent on ferrous iron-mediated oxidative stress, suggesting that drug resistance and ensuing tumor progression may in part stem from reduced ferroptosis. Since circular RNAs (circRNAs) have been shown to influence tumor development, we examined whether specific circRNAs may regulate druginduced ferroptosis in HCC. Through circRNA sequencing, we identified a novel hsa_circ_0000195 (circTTC13) that is overexpressed in HCC tissues. This overexpression is linked to higher tumor grade, more advanced tumor stage, decreased ferroptosis, and poorer overall survival. Overexpression of CircTTC13 in HCC cell lines and explant tumors was associated with increased proliferation rates, enhanced metastatic capacity, and resistance to sorafenib, while also inhibiting ferroptosis. Conversely, circTTC13 silencing reduced malignant characteristics and promoted ferroptosis. In silico analysis, luciferase assays, and fluorescence in situ hybridization collectively demonstrated that circTTC13 directly targets and reduces miR-513a-5p expression, which in turn leads to the upregulation of the negative ferroptosis regulator SLC7A11. Moreover, the inhibition of SLC7A11 mirrored the effect of circTTC13 knockdown, whereas ferroptosis inhibition mimicked the effect of circTTC13 overexpression. Both circTTC13 and SLC7A11 were highly expressed in drug-resistant HCC cells, and circTTC13 silencing induced ferroptosis and reversed sorafenib resistance in explant tumors. These findings identify circTTC13 as a critical driver of HCC progression and resistance to drug-induced ferroptosis via upregulation of SLC7A11. The cicTTC13/miR-513a-5p/ SLC7A11 axis represents a potential therapeutic target for HCC.

Keywords Hepatocellular carcinoma, Ferroptosis, circTTC13, SLC7A11, Sorafenib, circRNA, microRNA

[†]Ying Zhang, Ruiwei Yao, Mingyi Li, and Chongkai Fang contributed equally to this work.

*Correspondence: Chong Zhong zhongchong1732@gzucm.edu.cn

Full list of author information is available at the end of the article



© The Author(s) 2025. **Open Access** This article is licensed under a Creative Commons Attribution-NonCommercial-NoDerivatives 4.0 International License, which permits any non-commercial use, sharing, distribution and reproduction in any medium or format, as long as you give appropriate credit to the original author(s) and the source, provide a link to the Creative Commons licence, and indicate if you modified the licensed material. You do not have permission under this licence to share adapted material derived from this article or parts of it. The images or other third party material in this article are included in the article's Creative Commons licence, unless indicated otherwise in a credit line to the material. If material is not included in the article's Creative Commons licence and your intended use is not permitted by statutory regulation or exceeds the permitted use, you will need to obtain permission directly from the copyright holder. To view a copy of this licence, visit http://creativecommons.org/licenses/by-nc-nd/4.0/.

Zhang et al. Molecular Cancer (2025) 24:32 Page 2 of 18

Introduction

Hepatocellular carcinoma (HCC) constitutes 75–85% of primary liver cancer cases, making it the sixth most common and third most deadly malignancy worldwide [1]. Despite the growing number of treatment options, including immune checkpoint inhibitors, sorafenib, and lenvatinib, the objective response rate remains low due to variations in individual sensitivity, intolerable side effects, and progressive drug resistance [2–4]. Understanding the mechanisms driving HCC progression and treatment resistance is essential for identifying new and effective molecular targets for diagnosis and treatment.

Circular RNAs (circRNAs) are non-coding RNAs typically exhibiting tissue- or cell-type-specific expression. They are generated by the reverse splicing of premRNA, forming a covalently closed loop without a 5'-cap or 3'-poly(A) tail. Compared to linear RNA, circRNAs are not easily degraded by external enzymes and exhibit higher stability, suggesting their potential as biomarkers for cancer diagnosis and prognosis [5]. circRNAs perform various functions in organisms, such as acting as sponges for microRNAs (miRNAs) or proteins, or directly regulating transcription by interacting with RNA-binding proteins. Additionally, some circRNAs can be translated into proteins. miRNAs are post-transcriptional regulators of gene expression that function through direct base pairing with target sites within the untranslated regions of messenger RNAs. In 2007, Ebert et al. first reported the concept of a "miRNA sponge," which can inhibit miRNA activity in cells by competitively binding to miRNA target sites [6]. In 2013, Hansen et al. found that circRNA can act as a miRNA sponge for miR-7, containing more than 70 selectively conserved miRNA target sites, which can inhibit miR-7 activity and increase the levels of miR-7 downstream target genes [7]. Since then, numerous studies have shown that circRNAs can function as miRNA sponges and play roles in various cancers. Despite the numerous circRNAs differentially expressed in HCC, their potential roles in carcinogenesis and treatment response remain largely unexplored.

Recent studies have found that circRNAs can regulate lipid metabolism, which is closely related to the progression of HCC. Yang et al. discovered that circEPB41 is a circular RNA that promotes lipogenesis and mediates lipid metabolism in HCC [8]. Li et al. found that CircLARP1B affects HCC lipid metabolism and metastasis by regulating liver kinase B1 [9]. Dong et al. identified a new exosomal circUPF2, which regulates ferroptosis in HCC by targeting SLC7A11 [10]. SLC7A11 is a cystine/glutamate antiporter protein that transports extracellular cystine into the cytoplasm, where it is reduced to cysteine and subsequently used to synthesize glutathione for antioxidant defense [11]. In addition, several studies have shown that SLC7A11 is influenced by various genes

related to lipid metabolism. Therefore, regulating lipid metabolism can impact tumor ferroptosis [12, 13]. These studies have linked various circRNAs to liver cancer development and lipid metabolic pathways, highlighting their potential as therapeutic targets. This finding also underscores the potential of circRNAs in regulating ferroptosis. Ferroptosis is a form of programmed cell death that depends on free ferrous iron and the generation of reactive oxygen species (ROS), and it is closely related to lipid metabolism [14, 15]. Lipid peroxidation triggers the spread of lipid reactive oxygen species, which can oxidize lipid molecules on the cell membrane, thereby disrupting the integrity of cell membranes [16]. It can also damage the mitochondrial membrane, oxidize intracellular proteins, and cause oxidative damage to DNA molecules, ultimately resulting in cell death. Ferrous iron plays a key role in promoting phospholipid peroxidation, thereby enhancing ferroptosis. For instance, GPX4 prevents the formation of Fe²⁺-dependent ROS, and its inhibition leads to lipid peroxidation and induces ferroptosis [17]. ACSL4 is a lipid-metabolizing enzyme that promotes ferroptosis by facilitating the esterification of polyunsaturated fatty acids to acyl-CoA. Ferroptosis is frequently inhibited in tumor cells, allowing survival and growth even under stressful conditions [18]. Consequently, induction of ferroptosis has emerged as a promising cancer treatment strategy [19].

Tumor cells that are resistant to common chemotherapeutic drugs appear to be highly sensitive to ferroptosis inducers, suggesting that interventions for increasing ferroptosis sensitivity may also enhance the effectiveness of cancer treatments and potentially reverse acquired treatment resistance in advanced-stage disease [20]. Additionally, the regulation of lipid metabolism impacting ferroptosis in tumor cells may be crucial in reversing drug resistance, with circRNA potentially playing a significant role. Sorafenib is still the first-line treatment for advanced liver cancer patients, but resistance usually develops within six months, significantly diminishing its therapeutic efficacy [21]. Since cellular genes negatively regulating ferroptosis can confer sorafenib resistance [22], promoting ferroptosis may be an especially effective strategy for overcoming sorafenib-resistant HCC [23-26]. SLC7A11 is highly expressed in various cancer tissues, where it regulates cellular redox homeostasis, inhibits lipid peroxidation, influences ferroptosis [11], and consequently facilitates tumor progression and promotes drug resistance [27, 28].

In this study, we identified circTTC13 as a novel oncogenic factor that reduces HCC ferroptosis by enhancing SLC7A11 expression, leading to tumor growth and metastasis. Conversely, silencing circTTC13 reduced SLC7A11 expression and reversed sorafenib resistance by increasing ferroptosis. These findings identify circTTC13

Zhang et al. Molecular Cancer (2025) 24:32 Page 3 of 18

and SLC7A11 as regulators of HCC progression and potential therapeutic targets for preventing sorafenib resistance.

Materials and methods

Human specimens

Two experiments in this study utilized previously preserved human specimens. We first examined the differential expression of circRNAs by comparing expression profiles between 20 liver cancer tissue samples and corresponding adjacent non-tumor tissues. The second experiment analyzed the associations of specific circRNAs with patient prognosis using 80 liver cancer tissue samples. All specimens were obtained during hepatic cancer surgery at the First Affiliated Hospital of Guangzhou University of Chinese Medicine. The collection of these samples was approved by the Ethics Committee of the First Affiliated Hospital of Guangzhou University of Chinese Medicine, and all patients provided informed consent to participate in this study (Ethics Review No. K-2024-036).

Cell culture

Four human HCC cell lines, HepG2, Hep3B, MHCC97H, and Huh7, were used to examine the effects of circRNA expression on proliferation, migration, and metastatic capacity. All lines were obtained from the National Collection of Authenticated Cell Cultures and maintained in high-glucose Dulbecco's modified Eagle's medium (DMEM, Gibco, USA) supplemented with 10% fetal bovine serum(Gibco, USA) and 1% penicillin(Gibco, USA) – streptomycin mixture under a 5% $\rm CO_2/95\%$ air atmosphere at 37 °C. The non-cancerous human liver cell line THLE-2 was purchased from Wuhan Pricella Biotechnology and maintained under the same conditions in a specific medium provided by the supplier.

Isolation of stable sorafenib-resistant, circTTC13-knockdown, and circTTC13-overexpressing cell lines

To establish sorafenib-resistant cell lines, Hep3B cells were co-cultured with sorafenib starting at an initial concentration of half the maximum inhibitory concentration (IC50) and increasing by 0.5 μ M each week. Once the sorafenib concentration reached 10 μ M, the cells were continuously cultured and passaged in the presence of sorafenib for subsequent generations.

Transient transfection was carried out using the Lipofectamine 3000 kit (GlpBio, USA). When Hep3B cells reached 50% confluency, they were transfected with ov-NC, ov-SLC7A11, si-NC, and si-circTTC13. The overexpression plasmid for SLC7A11 and the small interfering RNAs (siRNAs) for circTTC13 were obtained from Beijing Tsingke Biotech Co., Ltd. (Beijing, China). Upon reaching 50% confluency, Hep3B/HepG2 cells were transfected with sh-circTTC13, sh-NC, ov-circTTC13, and

ov-NC lentiviruses. Transfected cells were selected using puromycin (2 μ g/mL, Amresco, USA). Stable transfection was performed using lentiviral vectors. The lentiviral vectors for circTTC13 knockdown and overexpression were sourced from OBiO Technology (Shanghai, China).

Real-time quantitative reverse transcription PCR(qRT-PCR)

Total RNA was extracted from the samples following complete lysis with Trizol reagent. The RNA was then reverse transcribed into cDNA using the Evo M-MLV reverse transcription reagent (Accurate Biology, Changsha, China). Reaction systems were set up for qRT-PCR to quantify circRNA or mRNA levels, utilizing SYBR Green reagent (Accurate Biology, Changsha, China).

Western blotting

After weighing 20 mg of frozen tissue or scraping fresh cells, RIPA lysate containing protease and phosphatase inhibitors was added. Cell samples were lysed, and the supernatants were removed by direct centrifugation. Protein concentration was determined according to the instructions of the BCA Protein Quantification kit. Subsequently, 5× protein sample buffer was added, and the samples were denatured by heating at 100 °C for 10 min. An SDS-PAGE gel was prepared, and equal amounts of protein were loaded. Following electrophoresis, membrane transfer, and blocking, the PVDF membrane was incubated overnight at 4 °C with primary antibodies against GAPDH (Bioss, Beijing, China) and SLC7A11 (Boster, USA). After washing, the PVDF membrane was incubated with a secondary antibody (Wanleibio, Shenyang, China) at room temperature for 1 h before imaging.

RNase R treatment assay

Total RNA was extracted using Trizol and digested with RNase R (GENESEED, Guangzhou, China). The samples were then reverse transcribed and analyzed by qRT-PCR.

Actinomycin D assay

Once the cells in the 6-well plates reached 70% confluence, 5 μ g/mL actinomycin D (GlpBio, USA) or DMSO as a control was added. The cells were then collected at five different time points: 0, 4, 8, 12, and 24 h. Total RNA was extracted, and reverse transcribed, and the CT values were calculated using qRT-PCR. The expression levels of the circTTC13 and TTC13 genes at different time points were determined.

Cell proliferation, migration, and metastasis assays

Colony Formation Assay: Hep3B cells stably transfected with sh-NC or sh-circTTC13 were seeded into 12-well culture plates at a density of 1×10^3 cells/well. After 14 days, the cells were fixed with 4%

Zhang et al. Molecular Cancer (2025) 24:32 Page 4 of 18

paraformaldehyde and stained with 0.1% crystal violet before being photographed.

Transwell Invasion Assays: DMEM medium was mixed with Matrigel gel (Corning, USA) at a ratio of 8:1 on ice and added to the upper chamber of the transwell insert for 6 h at 37 °C. Hep3B cells stably transfected with sh-NC or sh-circTTC13 were seeded into the upper chamber at a density of 1×10^5 cells/well. After 24 h of continued culture, the chambers were removed, and the cells were stained with crystal violet and photographed.

Wound-Healing Assay: Once the cells in the 6-well plates reached 80% confluence, they were scratched with 200 μ L pipette tips and photographed using Cytation5 (BioTek, USA). The cells were then cultured for 48 h at 5% CO₂ and 37 °C and photographed again to record the wound healing process.

Glutathione (GSH) and malondialdehyde(MDA) assay

GSH Assay: Tissue or cell samples were extracted using the GSH kit (Beyotime, Shanghai, China). Total glutathione detection solution was added and incubated at room temperature for 5 min, followed by mixing with NADPH solution and reacting for 25 min. The absorbance was measured at 412 nm. Simultaneously, the content of oxidized glutathione (GSSG) was determined as required. The formula used was: GSH = total glutathione - GSSG \times 2

MDA Assay: Tissue or cells were lysed using RIPA lysis buffer, and protein concentration was determined using the BCA Protein Quantification Kit. The samples were then added to the MDA working solution (Beyotime, Shanghai, China) to prepare them for testing. The MDA content was calculated by measuring the absorbance at 532 nm, and the initial MDA content was determined based on the protein content per unit weight or tissue weight.

MTT assay

Once the cells in the 96-well plates reached 70% confluence, various drugs (Ferrostatin-1, Z-VAD-FMK, Benacasan, Necrostatin-1, 3-Methyladenine, Sorafenib, MedChemExpress, USA) were applied for 24 h. The cell survival rate was then calculated by measuring the OD value at 490 nm after 4 h of continuous culture in a 9:1 mixture of DMEM and MTT medium.

Live/dead cell staining assay

Hep3B cells stably transfected with sh-NC or sh-circTTC13 were seeded in 96-well plates at a density of 5×10^3 cells/well for 48 h. Subsequently, 2 μM calcein AM and 8 μM PI (KeyGEN BioTECH, Jiangsu, China) were added and incubated in the dark for 30 min before being photographed.

5-Ethynyl-20-deoxyuridine (EdU) assay

Hep3B cells stably transfected with sh-NC or sh-circTTC13 were seeded in 96-well plates at a density of 5×10^3 cells/well. After 24 h, the cells were transfected with ov-SLC7A11 or ov-NC plasmids. Following another 24 h, EdU working solution (Beyotime, Shanghai, China) was added, followed by permeabilization solution, Click reaction solution, and Hoechst 33,342 solution. The cells were washed three times with washing solution before each addition of different liquids, and then photographed using Cytation5.

ROS, Fe²⁺ and mitochondrial membrane potential levels assay

DCFH - DA fluorescent probe: Hep3B cells stably transfected with sh-NC or sh-circTTC13 were seeded in 96-well plates at a density of 5×10^3 cells/well and incubated for 48 h. The medium was then replaced with a mixture of DCFH-DA (Beyotime, Shanghai, China) and DMEM at a ratio of 1:1000, and the cells were incubated in the dark for 20 min before being photographed.

FerroOrange fluorescent probe: Hep3B cells stably transfected with sh-NC or sh-circTTC13 were seeded in 96-well plates at a density of 5×10^3 cells/well. After 48 h of incubation, a 1 µmol/L concentration of FerroOrange (DOJINDO, Japan) fluorescent probe working solution was added. The cells were then incubated in the dark for 30 min before being photographed.

JC-1 fluorescent probe: Hep3B cells stably transfected with sh-NC or sh-circTTC13 were seeded in 96-well plates at a density of 5×10^3 cells/well. After 48 h, DMEM medium and JC-1 staining working solution (Beyotime, Shanghai, China) were added. The cells were incubated in the dark for 30 min and then washed with JC-1 staining buffer (1×).

Dual-luciferase reporter assay

Upon reaching 50% confluency, plasmids were added to the corresponding groups for the transfection of miR-485-3p, miR-513a-5p, circTTC13, and SLC7A11. After 48 h, the cells were treated with reporter gene cell lysate, and the supernatant was collected and added to a 96-well plate in the dark. Firefly luciferase detection reagent or Renilla luciferase detection reagent (Beyotime, Shanghai, China) were then added. The RLU value was measured after mixing.

Immunofluorescence assay and fluorescence in situ hybridization(IF-FISH)

After the cell slides were fixed in 4% paraformaldehyde, the cells were permeabilized with 0.1% Triton X-100. Probes for circTTC13 or miR-513a-5p (Umine Biotechnology Co., Ltd, Guangzhou, China) were hybridized with the hybridization solution for 16 h at 37 °C.

Zhang et al. Molecular Cancer (2025) 24:32 Page 5 of 18

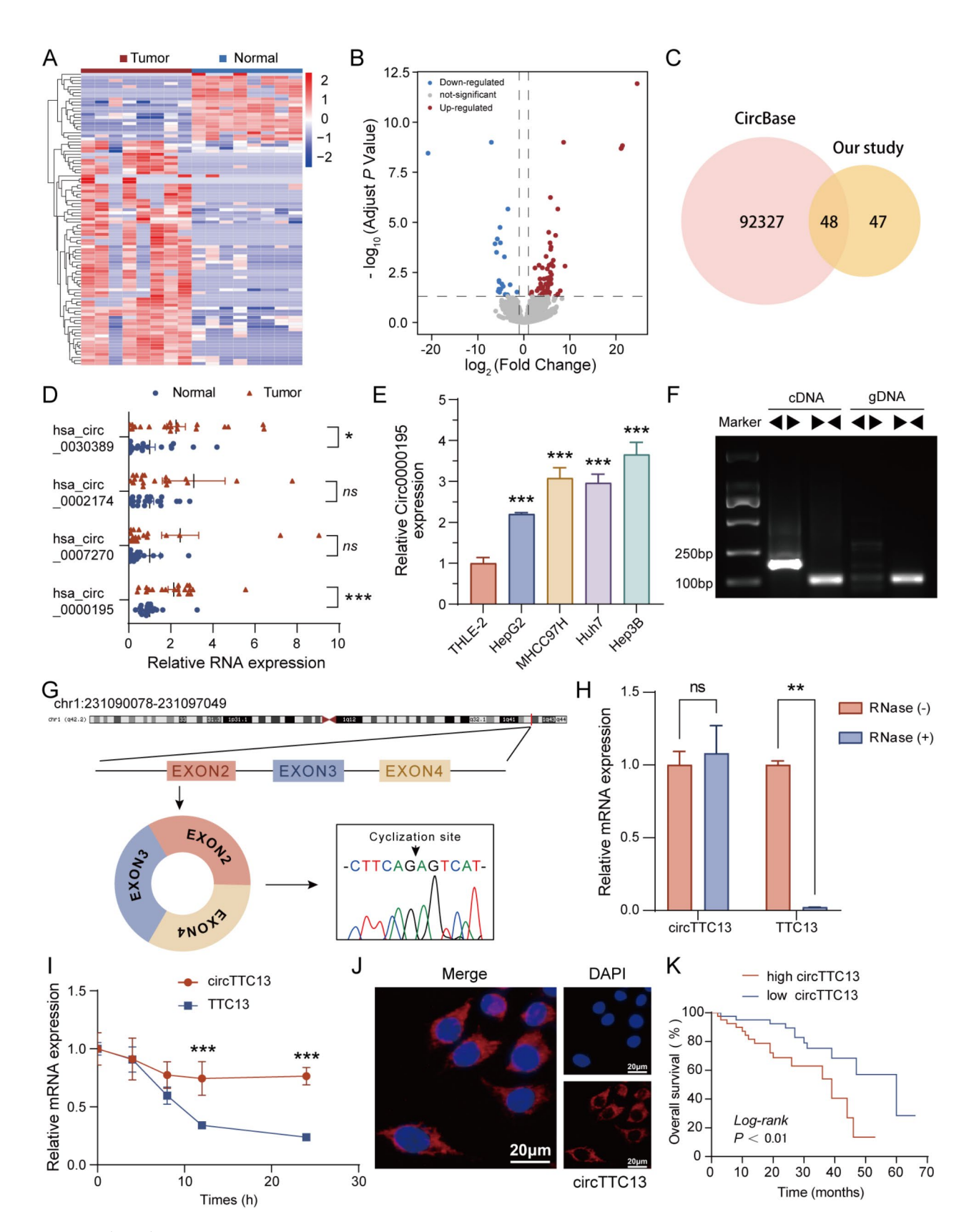


Fig. 1 (See legend on next page.)

Zhang et al. Molecular Cancer (2025) 24:32 Page 6 of 18

(See figure on previous page.)

Fig. 1 High expression of circTTC13 in HCC is associated with poor prognosis. (**A** & **B**) Heat map and volcano plot showing differentially expressed circRNAs between 8 HCC samples and adjacent non-cancerous tissues. (**C**) The intersection of differentially expressed circRNAs identified by sequencing with the circBase database. (**D**) Elevated expression levels of four candidate circRNAs in 20 HCC samples compared to adjacent non-cancerous tissues revealed by qRT-PCR. (**E**) Relative expression levels of circTTC13 in normal human liver cells and various HCC cell lines as measured by qRT-PCR. (**F**) CircTTC13 can be amplified by the divergent primers in cDNA, but not in gDNA. (**G**) Formation of circTTC13 (hsa_circ_0000195) by alternative splicing from exons 2–4 of the TTC13 gene. (**H**) Expression of circTTC13 and TTC13 gene in Hep3B cells was demonstrated by qRT-PCR following RNase R treatment qRT-PCR. (**I**) Stability of circTTC13 compared to TTC13 mRNA in Hep3B cells revealed by actinomycin D assay. (**J**) RNA-FISH showing circTTC13 localization in the cytoplasm of Hep3B cells. (**K**) Kaplan–Meier survival analysis showed that low circTTC13 expression is associated with longer overall survival of HCC patients. $^{ns}P > 0.05$, $^{**}P < 0.01$, $^{***}P < 0.001$

Following washing, the cells were blocked with a 5% BSA blocking solution and sequentially incubated with the SLC7A11 primary antibody and secondary antibody (Beyotime, Shanghai, China). After staining with DAPI, images of the cells were captured using a TCS SPE-II confocal microscope system (Leica, Germany).

Explant tumor models

All animal experiments were reviewed and approved by the Animal Ethics Committee of Guangzhou University of Chinese Medicine. Subcutaneous tumor model (Ethics Review No. 20230319001): NC or circTTC13 knockdown Hep3B cells were suspended at 2.5×10^7 /mL and 200 μL injected into the right axilla of BALB/C-nude mice. When subcutaneous tumors reached an average size of 50 mm³, mice were randomly divided into four treatment groups receiving intraperitoneal injection of 0.8 mg/kg Ferrostatin-1 or vehicle control daily for three weeks. Alternatively, mice were injected with the same number of CircTTC13-overexpressing or NC-overexpressing cells. Again, when tumors reached an average size of 50 mm³, mice were randomly divided into three groups and intraperitoneally injected with either 80 mg/kg sulfasalazine or a vehicle control daily for three weeks. In both trials, tumor volume was measured every three days.

Orthotopic model of hepatocellular carcinoma (Ethics Review No. 20240508008): To establish this model, circTTC13-knockdown Hep3B cells were suspended at $5\times10^7/\text{mL}$. Mice were anesthetized with an intraperitoneal injection of 2% sodium pentobarbital solution. After disinfection with iodophor, the liver was exposed, and 20 μ L of the cell suspension was slowly injected, followed by closure of the abdominal cavity. After four weeks, the mice were sacrificed under anesthesia, and the liver tissues were excised and collected for morphological analyses.

Sorafenib-Resistant Subcutaneous Tumor Model (Ethics Review No. 20240508008): To construct this model, sorafenib-resistant Hep3B-SR cells were suspended at $2.5 \times 10^7/\text{mL}$ and 200 mL injected into the the right axilla of BALB/C-nude mice. When the subcutaneous tumors reached an average size of 50 mm³, mice were randomly divided into two groups and intraperitoneally injected with either 20 mg/kg sorafenib or a vehicle control daily for three weeks. Alternatively, mice were divided into

two groups and injected with 20 mg/kg sorafenib plus circTTC13-target (5 nmol) or with sorafenib plus si-NC (5 nmol).

Immunohistochemistry (IHC)

Paraffin sections of tumor tissue were deparaffinized using xylene, dehydrated with a gradient of alcohol, and repaired under high pressure with EDTA. The sections were then immersed in 3% hydrogen peroxide for 10 minutes. Afterward, they were incubated overnight at 4°C with primary antibodies Ki-67 and 4-HNE (both from Abcam, USA). The next day, the sections were incubated with appropriate secondary antibodies (Jackson, USA) for 30 minutes at room temperature. Following color development with 3'-diaminobenzidine tetrahydrochloride, the sections were counterstained with hematoxylin, differentiated with alcohol hydrochloride, dehydrated with gradient alcohol, cleared with xylene, dried, and sealed with neutral tree glue. Photographs were taken using a Pannoramic MIDI digital slide scanning system (3DHISTECH, Hungary).

Statistical analyses

All results were analyzed using SPSS 22. Continuous variables meeting the criteria for normality and homogeneity of variance according to the Shapiro-Wilk test and Lenvene test were compared between two groups by independent sample t-tests or among multiple groups by one-way ANOVA with post hoc LSD tests. Continuous variables with a normal distribution but unequal variances were compared between two groups by two-sample paired t-test (t' test) or among multiple groups by Welch test with post hoc Games-Howell tests. Variables not following a normal distribution were compared by the Mann-Whitney U-rank sum test. Survival analysis was performed using the Kaplan–Meier method and compared by log-rank test. A *P* < 0.05 was considered statistically significant for all tests.

Results

CircTTC13 is elevated in HCC and associated with poor prognosis

To examine the potential contributions of novel circRNAs to HCC oncogenesis and progression, we first investigated differential expression of circRNAs between

Zhang et al. Molecular Cancer (2025) 24:32 Page 7 of 18

surgical HCC tissue samples and adjacent non-cancerous tissues (8 pairs). This analysis revealed 95 circRNAs with high differential expression between HCC and adjacent tissue, of which 22 were downregulated and 73 upregulated (Fig. 1A&B). By intersecting 95 differentially expressed circRNAs with all circRNAs of Homo sapiens species recorded in the circBase database, we selected the top 5 circRNAs with the highest expression in HCC or adjacent tissues. Among the 7 circRNAs identified (there were 3 duplicates), we chose 4 without prior functional studies and validated high expression in 20 additional clinical sample pairs. Ultimately, we identified hsa_circ_0000195 as differentially expressed in HCC (Fig. 1C&D). Overexpression of hsa_circ_0000195 was also confirmed in four human HCC cell lines (HepG2, Hep3B, MHCC97H, Huh7) compared to a normal human liver cell line (THLE-2) (Fig. 1E). Given that hsa_ circ_0000195 is most highly expressed in Hep3B cells and least expressed in HepG2 cells, we decided to knock down hsa_circ_0000195 in Hep3B cells and to overexpress it in HepG2 cells for subsequent functional validation (Figure S1A-D). PCR was conducted separately for cDNA and gDNA templates using divergent and convergent primers. The results indicated that TTC13 was amplified from both DNA templates, whereas

Table 1 Associations of circTTC13 expression level with the clinical characteristics of HCC

Variable	circTTC13		P
	High	Low	
Sex			1.000
male	31	30	
female	9	10	
Age, years			1.000
>50	27	28	
≤50	13	12	
TNM stage			0.176
T1a+T1b	19	26	
T2+T3	21	14	
BCLC stage			0.019
А	20	31	
B+C	20	9	
Edmondson's grade			0.013
+	13	25	
III + IV	27	15	
Number of tumors			0.222
solitary	25	31	
multiple	15	9	
Tumour size, mm			0.254
>50	19	13	
≤50	21	27	
vascular invasion			0.790
present	10	8	
absent	30	32	

hsa_circ_0000195 was present only in the cDNA template (Fig. 1F).

We subsequently characterized the fundamental properties of hsa_circ_0000195. This circRNA is generated by the circularization of exons 2-4 of the TTC13 gene through alternative splicing, with specific back-splicing confirmed via Sanger sequencing. Consequently, we refer to hsa circ 0000195 as circTTC13. The circular structure of circTTC13 was further validated through an RNase R treatment assay (Fig. 1H), and its stability was confirmed using an actinomycin D assay (Fig. 11). Fluorescence in situ hybridization (RNA-FISH) revealed that circTTC13 is predominantly located in the cytoplasm of Hep3B cells (Fig. 1J). We next showed that high circTTC13 expression is associated with poor HCC prognosis. A total of 80 clinical HCC samples were stratified into high and low circTTC13 expression groups based on qRT-PCR results and groups compared for overall survival (OS) using the Kaplan-Meier method (Fig. 1K). Overall survival was significantly longer in the patient group with lower circTTC13. Furthermore, correlation studies revealed positive associations between circTTC13 expression and both higher BCLC stage and Edmondson grade (Table 1). These findings suggest that elevated expression of circTTC13 is associated with the progression and lethality of HCC.

Silencing circTTC13 induces ferroptosis and inhibits the proliferation, invasion, and migration of liver cancer cells

To investigate the impact of circTTC13 on HCC prognosis, we initially assessed how changes in its expression affect cell proliferation, migration, and invasion capacity in vitro. Knockdown of circTTC13 by shRNA significantly inhibited HCC cell line proliferation as measured by viable colony formation assay, migration as evidenced by wound healing assay, and invasion as indicated by transwell assay (Fig. 2A-C). Thus, knocking down circTTC13 reduced key malignancy features. Moreover, live/dead cell staining showed that knocking down circTTC13 increased cell death (Fig. 2D), suggesting that reduced expression of circTTC13 may influence HCC cell death.

Treating Hep3B cells with the ferroptosis inhibitor Fer-1 at concentrations that did not significantly impact cell viability reversed the reduction in cell viability caused by circTTC13 silencing (Fig. 2E). In contrast, similar treatments with apoptosis inhibitor VZAD, necrosis inhibitor NEC-1, autophagy inhibitor 3-MA, or pyroptosis inhibitor BELNA had no such effect. This suggests that ferroptosis may be the primary mechanism by which circTTC13 influences HCC progression and treatment response. Therefore, we next investigated the correlation between circTTC13 expression and ferroptosis in HCC. We used electron microscopy to observe the changes in

Zhang et al. Molecular Cancer (2025) 24:32 Page 8 of 18

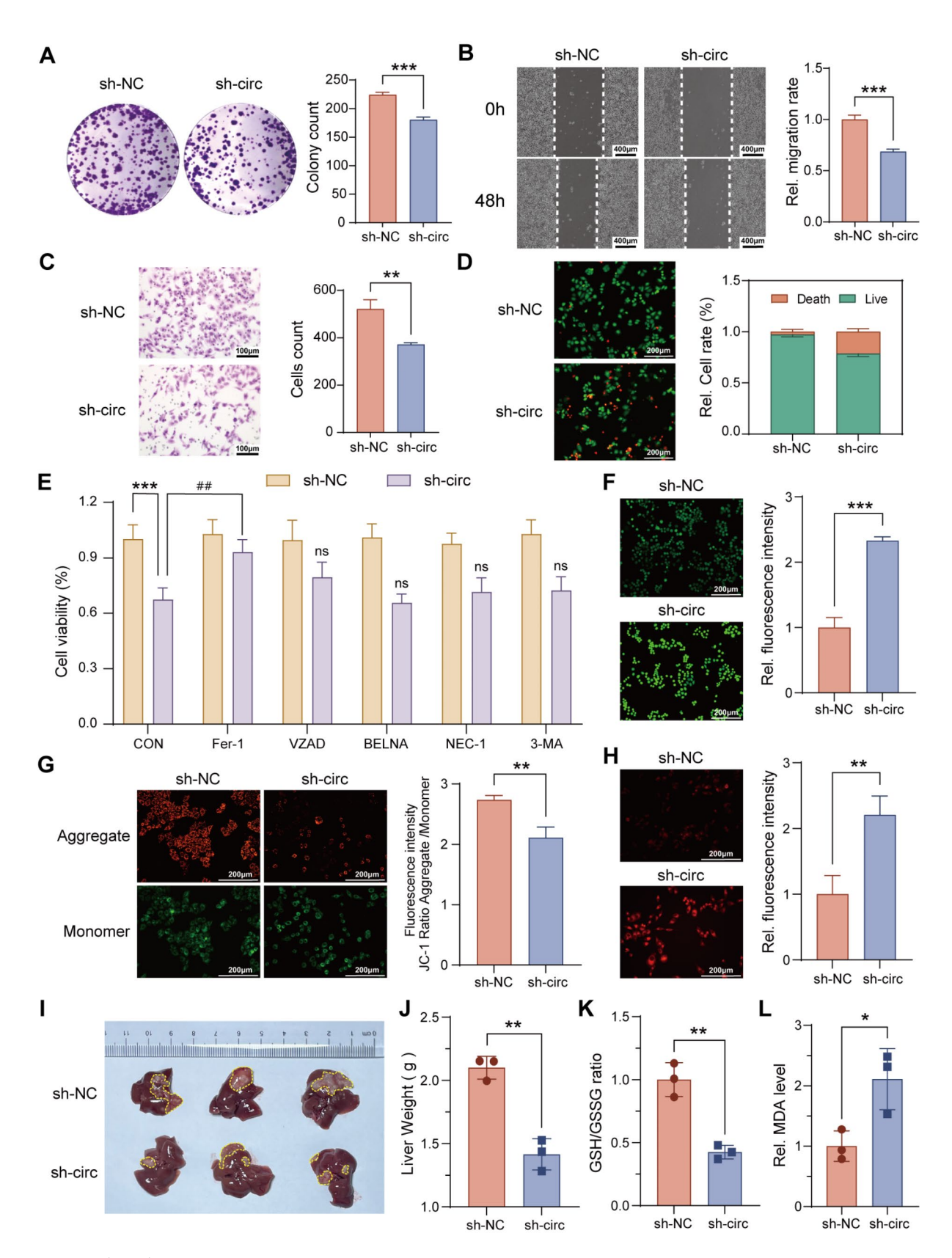


Fig. 2 (See legend on next page.)

Zhang et al. Molecular Cancer (2025) 24:32 Page 9 of 18

(See figure on previous page.)

Fig. 2 Silencing circTTC13 induces ferroptosis and inhibits the proliferation, invasion, and migration of liver cancer cells. **(A-D)** To examine the effects of circTTC13 expression level on malignancy behavior, Hep3B cells were transfected with either sh-NC or sh-circTTC13. Silencing circTTC13 expression reduced cell proliferation rate as evidenced by colony formation assay **(A)**, migration in the wound healing assay **(B)**, cell invasion in the transwell assay **(C)**, and live/dead cell ratio **(D)** compared to Hep3B cells transfected with sh-NC. **(E)** Ferroptosis inhibitor (Fer-1) reverses the effects of circTTC13 knockdown on cell viability. In contrast, neither the apoptosis inhibitor (VZAD), necrosis inhibitor (NEC-1), autophagy inhibitor (3-MA), nor pyroptosis inhibitor (BELNA) affected cell viability. **(F-H)** Knockdown of circTTC13 enhances ROS levels **(F)**, reduces mitochondrial membrane potential **(G)**, and increases Fe²⁺ levels **(H)** in Hep3B cells. **(I-L)** Orthotopic tumors in mouse liver seeded with circTTC13 knockdown Hep3B cells grow more slowly **(I, J)**, have lower glutathione (GSH) levels **(K)**, and exhibit higher MDA levels **(L)** compared to the sh-NC group. **P* < 0.05, ***P* < 0.01 and ****P* < 0.001 compared to the sh-NC group.

cells after knocking down circTTC13, and the results showed that the mitochondrial volume was reduced, cristae was reduced or disappeared, and the membrane density was slightly increased in the cytoplasmic part of Hep3B cells after knocking down circTTC13 (Figure S1E). Silencing the expression of circTTC13 significantly increased ROS accumulation (Fig. 2F), decreased mitochondrial membrane potential (Fig. 2G), increased Fe²⁺ levels (Fig. 2H), elevated ACSL4 protein expression, and reduced GPX4 protein expression (Figure S1F), all of which are consistent with increased ferroptosis. Additionally, the growth rate of mouse liver tumors derived from circTTC13-silenced HCC cells was significantly reduced compared to tumors seeded from normal HCC cells (Fig. 2I&J). Finally, tumors derived from circTTC13silenced HCC cells exhibited enhanced ferroptosis as evidenced by lower glutathione concentration and enhanced accumulation of lipid peroxides (Fig. 2K&L).

Silencing circTTC13 restricts the growth of explant HCC tumors by enhancing ferroptosis

To confirm the antitumorigenic effects of circTTC13 silencing and the role of ferroptosis in vivo, we established a subcutaneous tumor model in mice by seeding Hep3B cells expressing sh-NC (control) or sh-circTTC13 (silenced) and comparing tumor growth following treatment with vehicle or Fer-1. Silencing circTTC13 significantly decreased tumor volume and weight, effects that were partially reversed by Fer-1 injection (Fig. 3A-D). In addition, silencing circTTC13 suppressed HCC tumor progression (Fig. 3E&S2A), increased tissue ferrous iron levels (Figure S2B), downregulated the expression of the ferroptosis marker GPX4 and upregulated 4-hydroxynonenal (4-HNE), raised MDA levels, and promoted lipid peroxidation (Fig. 3F & S2C-E). Similarly, these effects were partially reversed by Fer-1. These results indicate that silencing circTTC13 promotes ferroptosis in vivo.

circTTC13 upregulates SLC7A11 by sponging miR-513a-5p

To investigate the mechanism of circTTC13 action, we initially knocked down circTTC13 to examine expression changes in the protein encoded by its parent gene. The results showed that circTTC13 knockdown almost did not affect TTC13 protein expression (Figure S2F). The physiological effects of circRNAs are often mediated by

binding to specific miRNAs (sponging), thereby removing the miRNA's inhibitory influence on mRNA translation. To investigate the specific mechanism by which circTTC13 regulates ferroptosis, we first searched for miRNAs with circTTC13 binding sites using the CircInteractome and CircBank databases and identified two potential candidates, miR-485-3p and miR-513a-5p (Fig. 4A&B). To verify the ability of these candidate miRNAs to bind circTTC13, we conducted luciferase activity assays in Hep3B cells co-transfected with wild-type or mutant circTTC13 and targeted miRmimic or NC-mimic. Luciferase activity did not differ between cells co-transfected with wild-type or mutant circTTC13 in the presence of miR-485-3p, whereas cotransfection of miR-513a-5p significantly reduced the luciferase activity of wild-type circTTC13 but not of mutant circTTC13(Fig. 4C&D). Additionally, RNA-FISH (Fig. 4E) demonstrated that circTTC13 colocalized with miR-513a-5p in the cytoplasm of Hep3B cells. These findings suggest that circTTC13 can bind to and sponge miR-513a-5p in the cytoplasm, thereby altering the expression of miR-513a-5p targets.

We next searched for downstream mRNA targets of miR-513a-5p using the Starbase, TargetScan, and miRDB databases. By intersecting candidates with the FerrDb database and genes related to ferroptosis from GeneCards, we identified 14 potential mRNA targets of miR-513a-5p and related to ferroptosis (Fig. 4F). Next, we used The Cancer Genome Atlas (TCGA) database to verify the differential expression of these 14 ferroptosis-related genes in HCC and tested each for prognostic significance using Cox regression, LASSO regression, the random forest algorithm, and Kaplan–Meier survival analysis. These analyses (Fig. 4G-K) indicated that among the 14 ferroptosis-related genes, high SLC7A11 expression was strongly associated with poor prognosis.

circTTC13 inhibits ferroptosis and promotes the proliferation, invasion, and migration of HCC through SLC7A11

We conducted dual-luciferase reporter assays and IF-FISH experiments to verify the interaction between miR-513a-5p and SLC7A11. Co-transfection of miR-513a-5p significantly reduced the luciferase activity of wild-type SLC7A11 but had no significant effect on the luciferase

Zhang et al. Molecular Cancer (2025) 24:32 Page 10 of 18

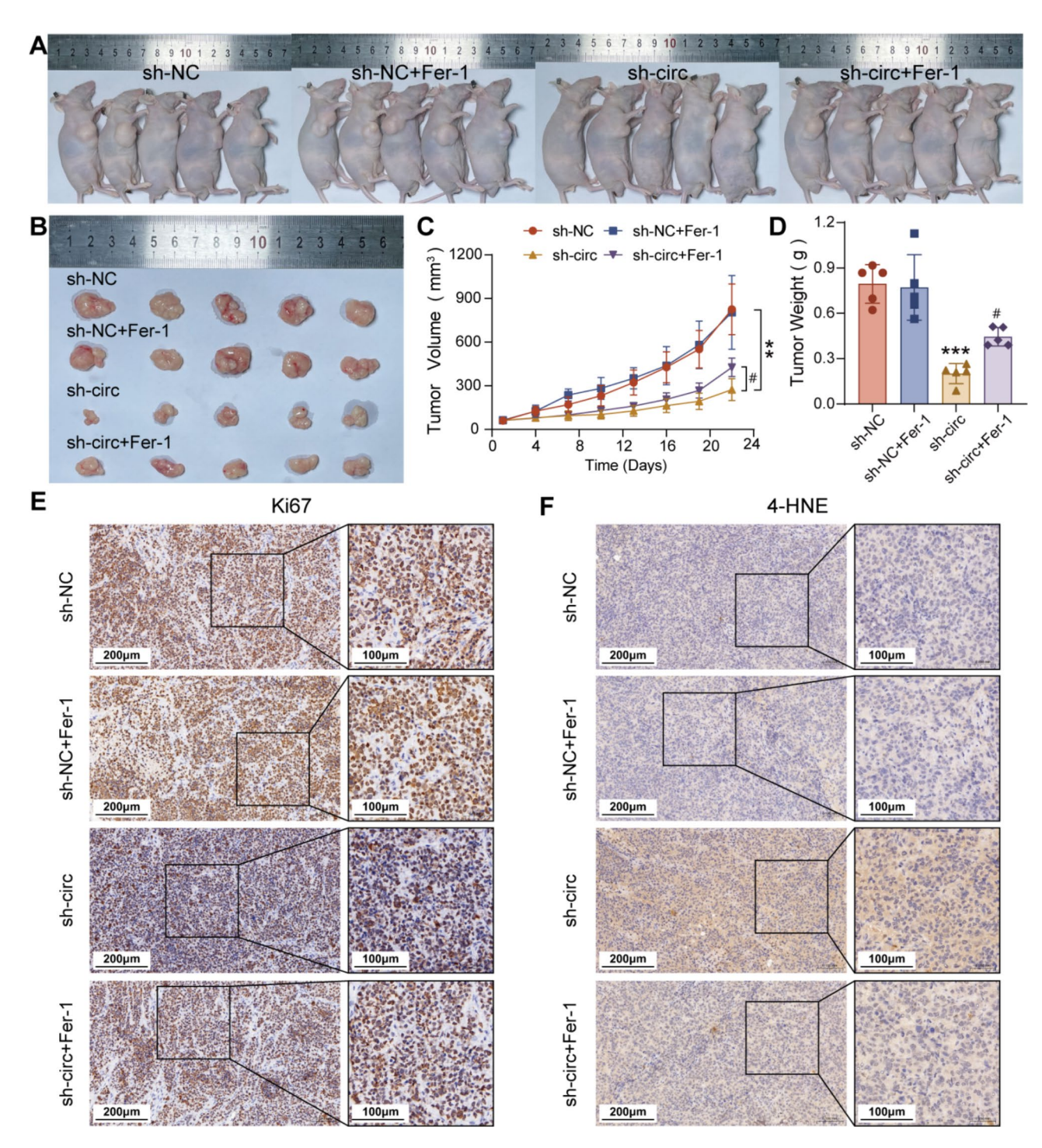


Fig. 3 Inhibition of ferroptosis reverses the anti-oncogenic effects of circTTC13 silencing in a mouse HCC model. BALB/c-nu mice were subcutaneously injected with Hep3B cells pre-transfected with sh-NC (control) or sh-circTTC13 (for silencing) and treated with the ferroptosis inhibitor Fer-1. (**A**) Images of subcutaneously transplanted tumor model mice showed no gross differences in body size across treatment groups. (**B**) Isolated tumors showing the anti-oncogenic effects of circTTC13 silencing. (**C**, **D**) Quantification of tumor volume (**C**) and mass (**D**). (**E**) Ki67 immunohistochemistry revealing proliferative cells. (**F**) Enhanced ferroptotic activity in tumors derived for circTTC13-silenced Hep3B cells as revealed by 4-HNE immunohistochemistry. **P<0.01 and ***P<0.001 versus the sh-NC group. P<0.05 versus the sh-circ group

Zhang et al. Molecular Cancer (2025) 24:32 Page 11 of 18

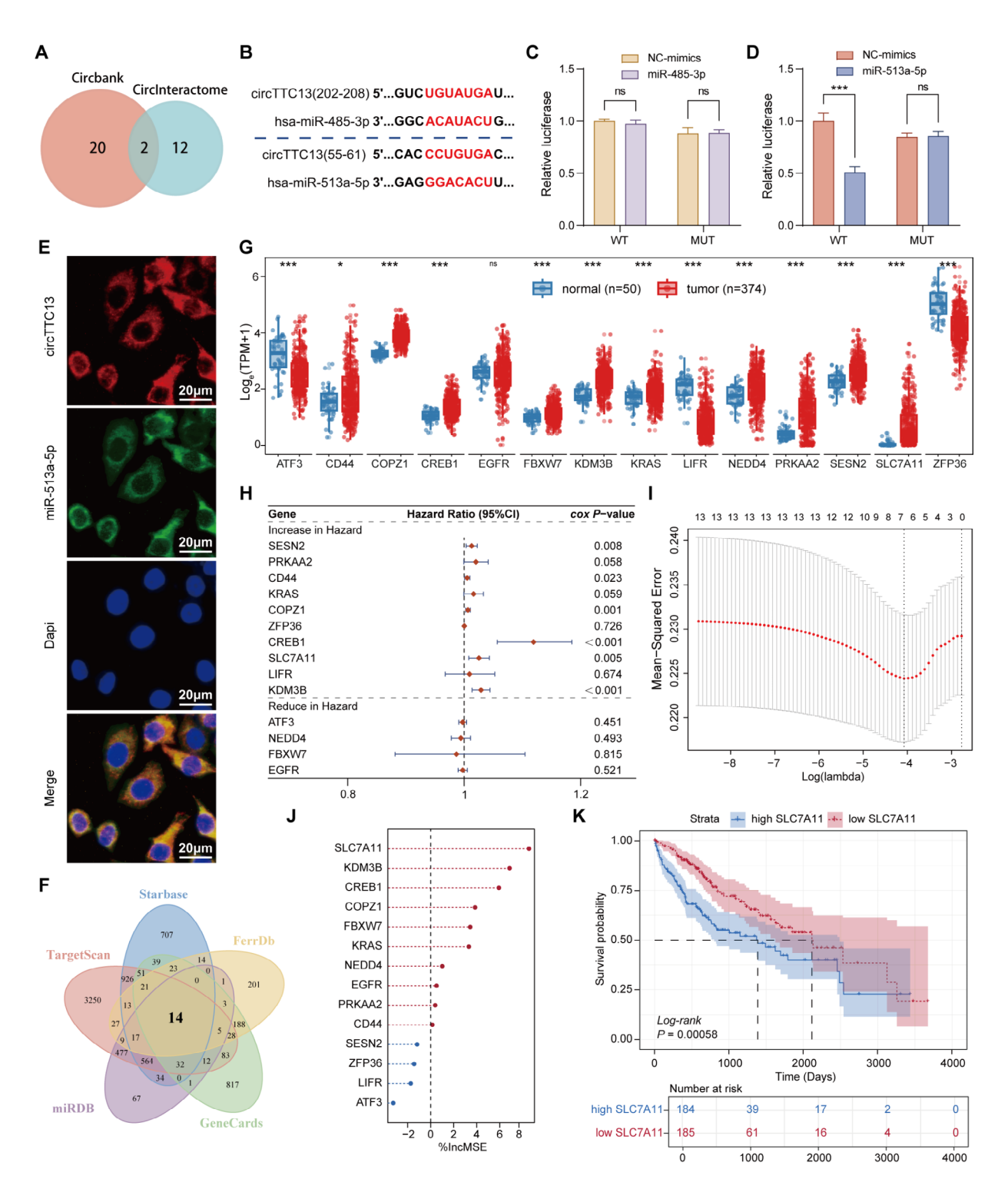


Fig. 4 circTTC13 sponges miR-513a-5p to upregulate SLC7A11. (**A**) Venn diagram illustrating miRNAs with potential binding sites for circTTC13. (**B**) Schematic diagram showing the binding sites of miR-485-3p and miR-513a-5p with hsa_circ_0000195 (circTTC13). (**C&D**) Luciferase activity of Hep3B cells co-transfected with miR-485-3p, miR-513a-5p, or NC-mimics plus wild type or mutant circTTC13. Co-transfection with miR-513a-5p but not miR-485-3p selectively and significantly reduces the luciferase activity of wild-type circTTC13 over mutant circTTC13. (**E**) RNA-FISH showing cellular co-localization of circTTC13 and miR-513a-5p. (**F**) Venn diagram showing 14 ferroptosis-related mRNAs with potential binding sites to miR-513a-5p identified through the intersection of Starbase, TargetScan, miRDB, FerrDb, and Genecard databases. (**G**) Expression levels of these 14 ferroptosis-related mRNAs in HCC tissues. (**H**-J) Prognostic Cox regression (**H**), LASSO regression (**I**), and random forest algorithm analysis(**J**) of these 14 ferroptosis-related mRNAs in HCC tissues. (**K**) Kaplan–Meier survival analysis of patients with different SLC7A11 expression levels. ^{ns}*P* > 0.05, **P* < 0.05, and *****P* < 0.001

Zhang et al. Molecular Cancer (2025) 24:32 Page 12 of 18

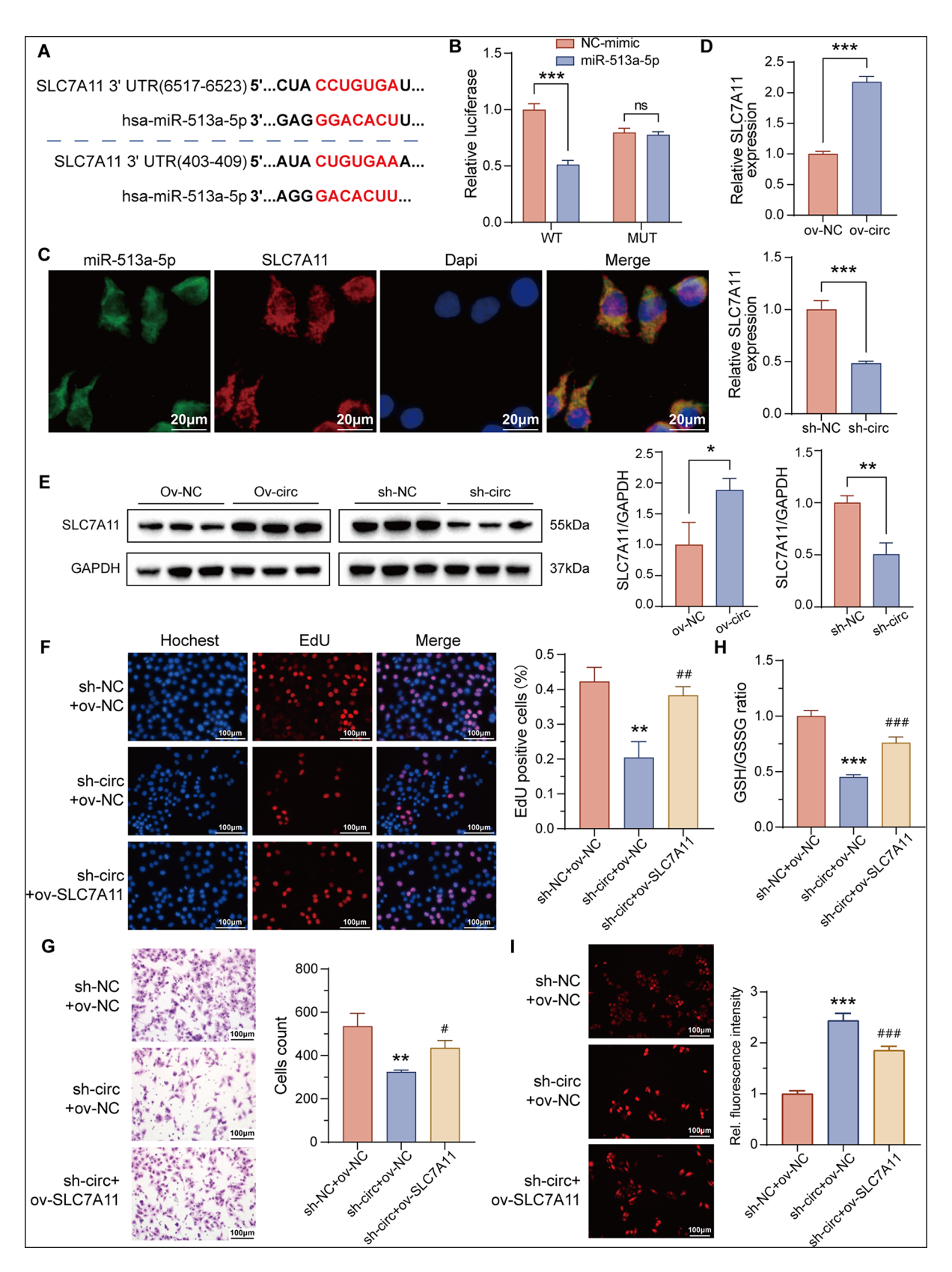


Fig. 5 (See legend on next page.)

Zhang et al. Molecular Cancer (2025) 24:32 Page 13 of 18

(See figure on previous page.)

Fig. 5 circTTC13 inhibits ferroptosis and promotes the proliferation, invasion, and migration of HCC through SLC7A11. (**A**) Schematic representation of the binding sites between SLC7A11 and miR-513a-5p. (**B**) Hep3B cells were co-transfected with either NC-mimic or miR-513a-5p and wild-type or mutant SLC7A11, and luciferase activity was measured. MiR-513a-5p significantly reduced the luciferase activity of wild type but not mutant SLC7A11. (**C**) Co-localization of miR-513a-5p and SLC7A11 in Hep3B cells was detected using an IF-FISH assay. (**D**&**E**) Overexpression of circTTC13 in HepG2 cells increases SLC7A11 gene and protein expression, while circTTC13 knockdown in Hep3B cells decreases it. (**F-I**) Overexpression of SLC7A11 reverses the effects of circTTC13 knockdown on Hep3B cell proliferation (**F**), invasion capacity (**G**), glutathione concentration (**H**), and ROS accumulation (**I**). ⁿ⁵P > 0.05, ^{*}P < 0.05, ^{**}P < 0.01, and ^{****}P < 0.001 versus WT/sh-NC/ov-NC/sh-NC+ov-NC group. [#]P < 0.01, and ^{****}P < 0.001 vs. sh-circ group

activity of mutant SLC7A11. MiR-513a-5p and SLC7A11 were co-localized primarily in the cytoplasm of Hep3B cells as evidenced by IF-FISH (Fig. 5A-C). Furthermore, clinical samples demonstrated a correlation between circTTC13 and SLC7A11 gene expressions (Figure S2G). Basal experiments also confirmed that the expression of SLC7A11 was significantly upregulated at both the gene and protein levels due to circTTC13 overexpression. Conversely, the knockdown of circTTC13 led to a significant downregulation of SLC7A11 gene and protein expression levels (Fig. 5D&E). Silencing circTTC13 inhibited the proliferation, invasion, reduced the protein expression of SLC7A11 and inhibited ferroptosis of HCC cells, while overexpression of SLC7A11 reversed these effects (Fig. 5F-I & S2H-J). Collectively, these findings suggest that the pro-oncogenic effects of circTTC13 result from miR-513a-5p sponging resulting in higher SLC7A11 expression.

A SLC7A11 inhibitor reversed the effects of circTTC13 overexpression on tumor growth

Next, we investigated whether the SLC7A11 inhibitor SSZ, at a concentration that did not significantly inhibit tumor growth on its own, could reverse the effects of circTTC13 overexpression on liver tumor growth and ferroptosis. Overexpression of circTTC13 significantly increased tumor volume and weight, and accelerated tumor progression (Fig. 6A-E & S3A), however, the concurrent downregulation of SLC7A11 protein reversed these effects. In addition, the regulation of ferroptosis by circTTC13 overexpression was also partially reversed by SSZ, as indicated by increased MDA accumulation and decreased GPX4 expression and GSH levels, which indicated promotion of ferroptosis (Fig. 6F-I and S3B). Moreover, to rule out the potential impact of SLC7A11 knockdown on tumor growth, we performed in vivo siRNA-mediated knockdown of SLC7A11 in tumors through local injections. Our findings revealed that knocking down SLC7A11 had a significantly greater inhibitory effect on tumor growth when circTTC13 was overexpressed compared to SLC7A11 knockdown alone. This suggests that circTTC13 may exert its effects via SLC7A11 (Figure S3C-F).

Silencing circTTC13 downregulates SLC7A11 and reverses sorafenib resistance

Cancer cells that are resistant to antineoplastic drugs are typically more sensitive to ferroptosis induction. Therefore, promoting ferroptosis could not only lower baseline survival but also increase the effectiveness of antineoplastic drugs. Therefore, we tested whether ferroptosis promotion via circTTC13 silencing reduces the antitumor drug resistance of HCC. For this purpose, we established a Hep3B cell line resistant to sorafenib, a classic firstline drug for liver cancer (Fig. 7A-D & S4A). CircTTC13 expression was significantly higher in these resistant cells compared to the parental cells (Fig. 7E). Moreover, knockdown of circTTC13 in resistant cells notably reduced cell viability and triggered ferroptosis (Fig. 7F & S4B-F). Moreover, circTTC13 knockdown reduced the volume and weight of tumors derived from drug-resistant Hep3B cells (Fig. 7G-I & S4G). Tumors with circTTC13 knockdown exhibited elevated levels of 4-HNE, increased ferrous iron and MDA levels, and reduced GSH levels in vivo (Fig. 7J & S4H-K). These findings suggest that circTTC13 knockdown may reverse sorafenib resistance by inducing ferroptosis. Finally, SLC7A11 expression was higher in sorafenib-resistant HCC cells and tissues, and was suppressed when circTTC13 was knocked down (Fig. 7K & S4L), consistent with the notion that silencing circTTC13 enhances sorafenib sensitivity and ferroptosis by downregulating SLC7A11.

Discussion

It has been nearly 50 years since circRNA was first discovered. Initially mistaken for viral-like pathogens [29], circRNAs have since been identified in viruses, prokaryotes, unicellular eukaryotes, and throughout the animal kingdom, including mammals [30], suggesting essential and well-conserved functions in gene regulation. The unique structure of circRNAs allows them to evade exonuclease degradation, resulting in a longer half-life (exceeding 48 h) and greater stability than linear RNAs [31]. These properties enable unique physiological and pathological functions. Notably, circRNAs are implicated in the development and progression of various malignant tumors [32] and may serve as predictive biomarkers and even therapeutic targets [33]. In the current study, high-throughput sequencing for circRNAs specifically expressed in clinical HCC samples revealed that circTTC13 was both highly expressed and

Zhang et al. Molecular Cancer (2025) 24:32 Page 14 of 18

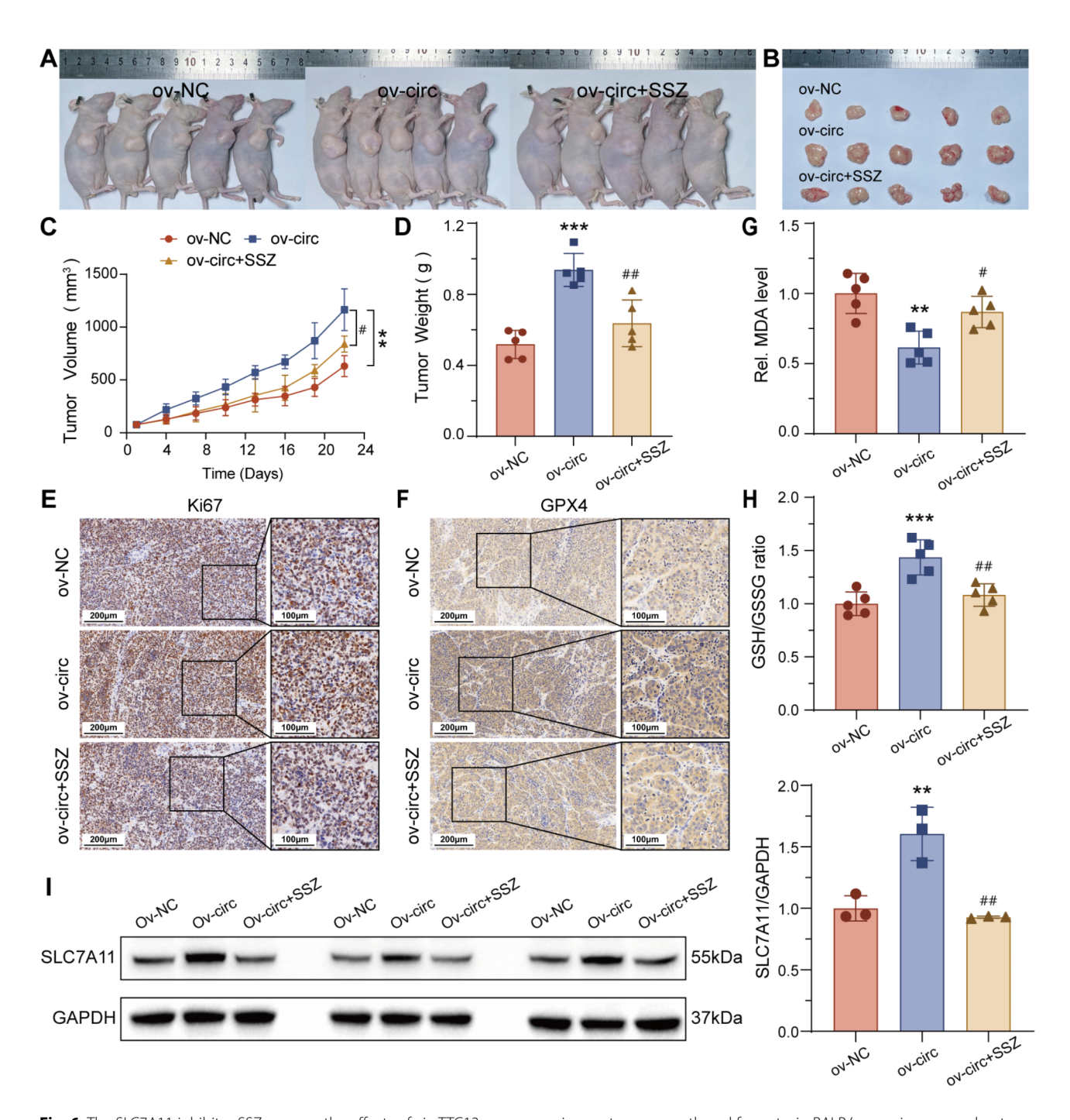


Fig. 6 The SLC7A11 inhibitor SSZ reverses the effects of circTTC13 overexpression on tumor growth and ferroptosis. BALB/c-nu mice were subcutaneously injected with HepG2 cells pre-transfected with either ov-NC or ov-circTTC13 and treated in vivo with the SLC7A11 inhibitor SSZ. (**A**) Images of tumor model mice from the different groups. (**B**) Excised tumors from the different treatment groups. (**C**, **D**) Group differences in tumor volume (**C**) and tumor weight (**D**). (**E**) Ki67 immunohistochemistry showing group difference in cell proliferation. (**F**) GPX4 immunohistochemistry showing group difference in ferroptosis. (**G-I**) Group differences in tumoral MDA accumulation (**G**), GSH (**H**), and SLC7A11 protein expression (**I**). **P<0.01 and ***P<0.001 versus the ov-NC group. *P<0.05 and **P<0.01 versus the ov-circ group

strongly associated with advanced pathological grade and tumor stage as well as poor overall survival. Ferroptosis, a form of iron-dependent cell death, is also a promising target for HCC as it may both slow basal growth and enhance the effectiveness of antitumor drugs. Differential expression of circRNAs in malignant tumors has been shown to regulate ferroptosis during cancer treatment. For instance, the highly expressed circRNF10 in glioblastoma was reported to trigger a positive feedback loop that mitigated ferroptosis and promoted

Zhang et al. Molecular Cancer (2025) 24:32 Page 15 of 18

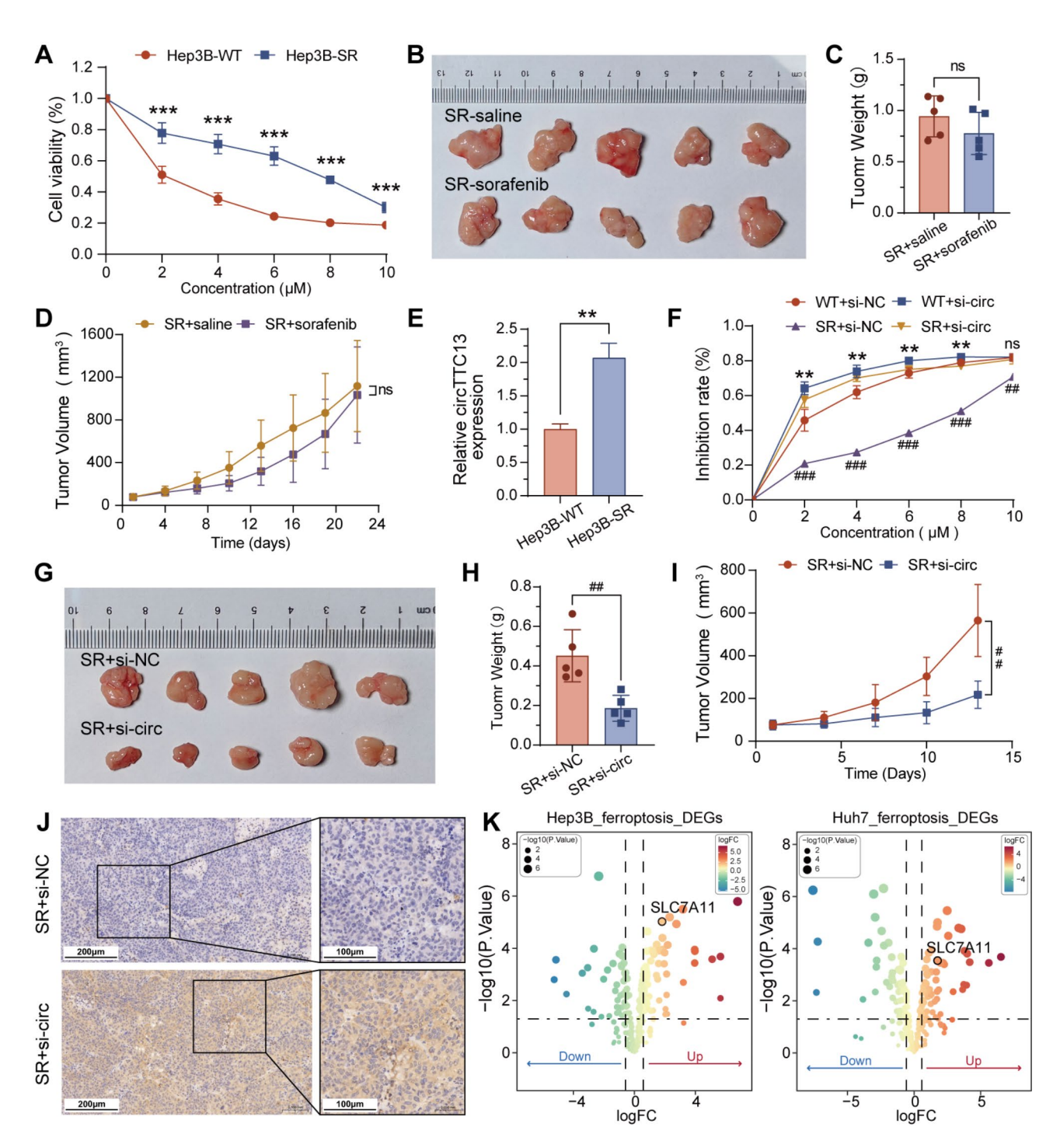


Fig. 7 Silencing circTTC13 downregulates SLC7A11 and reverses tumor sorafenib resistance. (**A**) Cell viability assay confirming the establishment of sorafenib-resistant Hep3B cells, which were subcutaneously transplanted to produce sorafenib-resistant tumors. (**B**) Diagram of the subcutaneous xenograft tumors. (**C**, **D**) Group differences in tumor weight (**C**) and volume (**D**). (**E**) CircTTC13 is highly expressed in sorafenib-resistant cells. (**F**) CircTTC13 knockdown reduces the viability of sorafenib-resistant cells. (**G**-J) CircTTC13 knockdown in tumors derived from sorafenib-resistant Hep3B cells (**G**) reduces tumor weight (**H**) and volume (**I**) and enhances 4-HNE immunoexpression (**J**). (**K**) Volcano plot from the GSE158458 database showing elevated SLC7A11 expression in drug-resistant cells. $^{ns}P > 0.05$, $^{**}P < 0.01$ and $^{***}P < 0.001$ versus the Hep3B-WT/SR+saline/WT+si-NC group. $^{##}P < 0.01$ and $^{##}P < 0.001$ versus the SR+si-NC group

Zhang et al. Molecular Cancer (2025) 24:32 Page 16 of 18

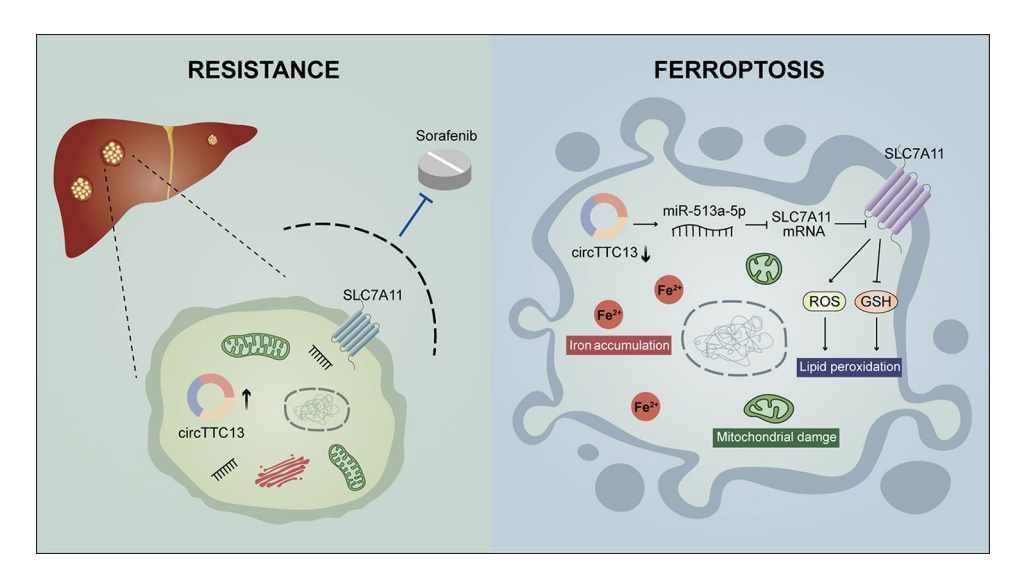


Fig. 8 CircTTC13 promotes sorafenib resistance in hepatocellular carcinoma through the inhibition of ferroptosis by targeting the miR-513a-5p/SLC7A11 axis

tumor progression [34]. Alternatively, downregulation of hsa_circ_0001546 in ovarian cancer was found to induce ferroptosis and inhibit the peritoneal metastasis of epithelial ovarian cancer by promoting the formation of an hsa_circ_0001546/14–3–3/CAMK2D/Tau complex [35]. Similarly, the knockdown of circTTC13 significantly inhibited HCC progression and promoted ferroptosis in mice, thereby reversing resistance to sorafenib.

CircRNAs regulate gene expression by altering transcription [36], targeting protein translation [37], and by acting as a miRNA sponge [38]. More than half of the studies on circRNA over the past decade have found that circRNAs regulate tumorigenesis by binding to specific miRNAs or proteins. Downstream effects of this binding include tumor drug resistance, changes in tumor metabolism, immune escape, and ferroptosis [39–42]. Given that miRNA sponging is the most common regulatory mechanism of cytoplasmic circRNAs [43], we screen for sponging targets associated with ferroptosis and identified miR–513a–5p, which targets the ferroptosis-negative regulator SLC7A11.

SLC7A11 is a cystine/glutamate antiporter protein that contributes to antioxidant defense by transporting extracellular cystine into the cytoplasm. Once inside the cell, cystine is reduced to cysteine, which is then used to synthesize the endogenous antioxidant glutathione (GSH) [44]. As a negative regulator of ferroptosis, SLC7A11 plays a crucial role in maintaining cellular redox homeostasis and is highly expressed in various cancer cells, impacting tumor growth [45], metastasis [46], drug resistance [47], and the effectiveness of anti-tumor treatments [48, 49]. We found that circTTC13 overexpression promoted tumor growth in mice and led to higher GSH levels and reduced lipid peroxidation, and these

effects were reversed by SLC7A11 inhibitors. Additionally, both circTTC13 and SLC7A11 were highly expressed in sorafenib-resistant cells, and the knockdown of circTTC13 reversed this resistance. In general, SLC7A11 inhibition paralleled the effect of circTTC13 knockdown while ferroptosis inhibition paralleled the effect of circTTC13 overexpression. Collectively, these findings indicate that the anti-ferroptotic effects of circTTC13 in HCC are mediated by the upregulation of SLC7A11.

The significant role of ferroptosis in tumor growth and drug resistance positions it as a promising strategy for cancer treatment. Recent discoveries highlight circTTC13's involvement in regulating ferroptosis, offering new insights for liver cancer therapy. Firstly, knocking down circTTC13 directly induces ferroptosis in liver cancer cells by impacting the cellular REDOX balance. circTTC13 acts as a sponge for miR-513a-5p, influencing SLC7A11 expression. When circTTC13 is knocked down, lipid peroxidation is induced by inhibiting SLC7A11 expression. This process suppresses GPX4 within the antioxidant system, reducing GSH levels, and leading to the accumulation of oxidative products like ROS and MDA. Additionally, circTTC13 knockdown causes iron accumulation in cells, which results in irondependent damage to membrane lipids and ultimately cell death. Secondly, HCC cells can develop resistance to sorafenib by downregulating ferroptosis to mitigate oxidative stress. However, inducing ferroptosis can counteract this resistance (Fig. 8).

In conclusion, our findings indicate that the novel circRNA circTTC13 is highly expressed in HCC, with its regulation of ferroptosis being closely linked to HCC progression and poor prognosis. This study provides compelling evidence for the potential of circTTC13 as a

Zhang et al. Molecular Cancer (2025) 24:32 Page 17 of 18

biomarker and therapeutic target for HCC. However, our research primarily focused on the role of circTTC13 in regulating ferroptosis in HCC and its underlying mechanisms. The specific target of circTTC13 in sorafenib resistance was not fully verified. Additionally, questions remain about whether circTTC13 can regulate resistance to other drugs and if combining circTTC13 with first-line targeted immunotherapy for liver cancer could yield better efficacy. These questions warrant further investigation and hold significant promise for future research.

Supplementary Information

The online version contains supplementary material available at https://doi.org/10.1186/s12943-024-02224-3.

Supplementary Material 1: Figure S1 (A&B) Stable circTTC13 knock-down cell line was established in Hep3B cells using lentivirus. Compared to the control stable Hep3B cell line, the expression level of circTTC13 was significantly lower in the stable Hep3B cell line carrying the target gene. (C&D) Stable circTTC13 overexpression cell line was established in HepG2 cells using lentivirus. Compared to the control stable HepG2 cell line, the expression level of circTTC13 was significantly higher in the stable HepG2 cell line carrying the target gene. (E) To examine the cell ultrastructure using electron microscopy, Hep3B cells were transfected with either sh-NC or sh-circTTC13. (F) To assess changes in ACSL4 and GPX4 protein levels, Hep3B cells were transfected with either sh-NC or sh-circTTC13. *P < 0.05, ***P < 0.001. Figure S2 (A-E) BALB/c-nu mice were subcutaneously injected with Hep3B cells pre-transfected with sh-NC (control) or sh-circTTC13 (for silencing) and treated with the ferroptosis inhibitor Fer-1. (A) Statistical analysis of Ki67 immunohistochemistry. (B) The content of ferrous iron in tumor tissues. (C) The content of MDA in tumor tissues. (D) Statistical analysis of 4HNE immunohistochemistry. (E) GPX4 immunohistochemistry showing group difference in ferroptosis. (F) To assess changes in TTC13 protein levels, Hep3B cells were transfected with either sh-NC or sh-circTTC13. (G) Correlation analysis of circTTC13 and SLC7A11 gene expressions in 80 clinical HCC tissues. (H-J) Overexpression of SLC7A11 reverses the effects of circTTC13 knockdown on SLC7A11 protein levels (H), MDA accumulation (I) and lipid peroxidation levels (J) in Hep3B cells. $^{ns}P > 0.05, ^{**}P < 0.01$ and $^{***}P < 0.001$ versus sh-NC/sh-NC + ov-NC group. $^{\#}P$ < 0.05, ***P < 0.01, and ****P < 0.001 versus sh-circ/sh-circ + ov-NC group. Figure S3 (A&B) BALB/c-nu mice were subcutaneously injected with HepG2 cells pre-transfected with either ov-NC or ov-circTTC13, and treated in vivo with the SLC7A11 inhibitor SSZ. Statistical analysis was performed on Ki67 (A) and GPX4 (B) immunohistochemistry. (C-F) BALB/c-nu mice were subcutaneously injected with HepG2 cells pre-transfected with either ov-NC or ov-circTTC13, and treated in vivo with SLC7A11 siRNA knockdown. (C) Images of tumor model mice from the different groups. (D) Excised tumors from the different treatment groups. (E&F) Group differences in tumor volume (E) and tumor weight (F). $^{ns}P > 0.05$, $^*P < 0.05$ and $^{***}P <$ 0.001 versus ov-NC/ov-NC + si-NC group. ***P < 0.01 and ****P < 0.001 versus ov-circ/ov-circ + si-NC group. Figure S4 (A) Images of tumor model mice from the SR-saline and SR-sorafenib groups. (B-F) Knockdown of circTTC13 increases MDA accumulation (B), decreases GSH levels (C), and elevates ROS (D), Fe²⁺ (E), and lipid peroxidation levels (F) in sorafenib-resistant Hep3B cells. (G) Images of tumor model mice from the SR + si-NC and SR + si-circ groups. (H-K) Knockdown of circTTC13 in tumors derived from sorafenib-resistant Hep3B cells led to increased levels of 4-HNE (H), ferrous iron (I), and MDA (J), while decreasing GSH levels (K). (L) Knockdown of circTTC13 downregulates SLC7A11 levels in sorafenib-resistant Hep3B tissues. **P < 0.01 and ***P < 0.001.

Author contributions

C Z, Y Z conceived and designed the experiments. Y Z, R-W Y, M-Y L, X-R C, K-L F, J-N W, and X-L Z performed the experiments. Y Z, R-W Y, R L, H-Q S, and X-Q C performed the statistical collection and analysis. Y Z, R-W Y, M-Y L, H-L H, S-W

 $\mathsf{L},\mathsf{B}\,\mathsf{Y},\mathsf{and}\,\mathsf{C}\text{-}\mathsf{K}\,\mathsf{F}$ wrote the manuscript. All authors read and approved the final manuscript.

Funding

This work was supported by the National Natural Science Foundation of China [NSFC 82274526]; Natural Science Foundation of Guangdong Province, China [2023A1515011069]; Quality Enhancement Program of Guangzhou University of Chinese Medicine [A1-2601-24-415-110Z41]; Cultivation Program for Disciplinary Reserve Talents of Guangzhou University of Chinese Medicine [A1-2601-22-415-023].

Data availability

No datasets were generated or analysed during the current study.

Declarations

Ethical approval

All specimens in this study were obtained during hepatic cancer surgery at the First Affiliated Hospital of Guangzhou University of Chinese Medicine. The collection of these samples was approved by the Ethics Committee of the First Affiliated Hospital of Guangzhou University of Chinese Medicine, and all patients provided informed consent to participate in this study (Ethics Review No. K-2024-036). This study and included experimental procedures were approved by the Experimental Animal Ethics Committee of Guangzhou University of Chinese Medicine. All animal housing and experiments were conducted in strict accordance with the institutional guidelines of laboratory animals (Ethics Review No. 20230319001, No. 20240508008, No. 20240508008, No. 20241009011).

Competing interests

The authors declare no competing interests.

Author details

¹State Key Laboratory of Traditional Chinese Medicine Syndrome/The First Affiliated Hospital of Guangzhou University of Chinese Medicine, Guangzhou University of Chinese Medicine, Guangzhou, China ²Shenzhen Bao'an Chinese Medicine Hospital, Guangzhou University of Chinese Medicine, Shenzhen, China

³Department of Biliary-Pancreatic Surgery, The First Affiliated Hospital of Guangzhou University of Chinese Medicine, Guangzhou, China ⁴First Clinical Medical College, Guangzhou University of Chinese Medicine, Guangzhou, China

⁵Lingnan Medical Research Center, Guangzhou University of Chinese Medicine, Guangzhou, China

⁶The 3rd Ward of Radiotherapy Department, Guangzhou Institute of Cancer Research, the Affiliated Cancer Hospital, Guangzhou Medical University, Guangzhou, China

⁷Science and Technology Innovation Center, Guangzhou University of Chinese Medicine, Guangzhou, China

⁸Department of Surgery, Baiyun Hospital of the First Affiliated Hospital of Guangzhou University of Chinese Medicine, Guangzhou, China

Received: 17 August 2024 / Accepted: 31 December 2024 Published online: 27 January 2025

References

- Bray F, Laversanne M, Sung H, et al. Global cancer statistics 2022: GLOBOCAN estimates of incidence and mortality worldwide for 36 cancers in 185 countries [J]. CA Cancer J Clin. 2024;74(3):229–63.
- Vogel A, Meyer T, Sapisochin G, et al. Hepatocellular carcinoma [J]. Lancet. 2022;400(10360):1345–62.
- Yang C, Zhang H, Zhang L, et al. Evolving therapeutic landscape of advanced hepatocellular carcinoma [J]. Nat Rev Gastroenterol Hepatol. 2023;20(4):203–22.
- Wang Z, Wang Y, Gao P, et al. Immune checkpoint inhibitor resistance in hepatocellular carcinoma [J]. Cancer Lett. 2023;555:216038.
- Lei B, Tian Z, Fan W, et al. Circular RNA: a novel biomarker and therapeutic target for human cancers [J]. Int J Med Sci. 2019;16(2):292–301.

Zhang et al. Molecular Cancer (2025) 24:32 Page 18 of 18

- Ebert MS, Neilson JR, Sharp PA. MicroRNA sponges: competitive inhibitors of small RNAs in mammalian cells [J]. Nat Methods. 2007;4(9):721–6.
- Hansen TB, Jensen TI, Clausen BH, et al. Natural RNA circles function as efficient microRNA sponges [J]. Nature. 2013;495(7441):384–8.
- 8. Yang Y, Luo J, Wang Z et al. Energy stress-induced CircEPB41(2) promotes lipogenesis in Hepatocellular Carcinoma [J]. Cancer Res, 2024.
- Li J, Wang X, Shi L, et al. A mammalian conserved circular RNA CircLARP1B regulates hepatocellular carcinoma metastasis and lipid metabolism [J]. Adv Sci (Weinh). 2024;11(2):e2305902.
- Dong FL, Xu ZZ, Wang YQ, et al. Exosome-derived circUPF2 enhances resistance to targeted therapy by redeploying ferroptosis sensitivity in hepatocellular carcinoma [J]. J Nanobiotechnol. 2024;22(1):298.
- Yan Y, Teng H, Hang Q, et al. SLC7A11 expression level dictates differential responses to oxidative stress in cancer cells [J]. Nat Commun. 2023;14(1):3673.
- Li Y, Yang W, Zheng Y, et al. Targeting fatty acid synthase modulates sensitivity
 of hepatocellular carcinoma to sorafenib via ferroptosis [J]. J Exp Clin Cancer
 Res. 2023;42(1):6.
- Sun R, Lin Z, Wang X, et al. AADAC protects colorectal cancer liver colonization from ferroptosis through SLC7A11-dependent inhibition of lipid peroxidation [J]. J Exp Clin Cancer Res. 2022;41(1):284.
- 14. Tang D, Kroemer G, Kang R. Ferroptosis in hepatocellular carcinoma: from bench to bedside [J]. Hepatology. 2024;80(3):721–39.
- 15. Yang S, Hu C, Chen X, et al. Crosstalk between metabolism and cell death in tumorigenesis [J]. Mol Cancer. 2024;23(1):71.
- 16. Cheng C, Geng F, Cheng X, et al. Lipid metabolism reprogramming and its potential targets in cancer [J]. Cancer Commun (Lond). 2018;38(1):27.
- Forcina GC, Dixon SJ. GPX4 at the crossroads of lipid homeostasis and ferroptosis [J]. Proteomics. 2019;19(18):e1800311.
- Balihodzic A, Prinz F, Dengler MA, et al. Non-coding RNAs and ferroptosis: potential implications for cancer therapy [J]. Cell Death Differ. 2022;29(6):1094–106.
- Dixon SJ, Lemberg KM, Lamprecht MR, et al. Ferroptosis: an iron-dependent form of nonapoptotic cell death [J]. Cell. 2012;149(5):1060–72.
- Zhang C, Liu X, Jin S, et al. Ferroptosis in cancer therapy: a novel approach to reversing drug resistance [J]. Mol Cancer. 2022;21(1):47.
- Tang W, Chen Z, Zhang W, et al. The mechanisms of sorafenib resistance in hepatocellular carcinoma: theoretical basis and therapeutic aspects [J]. Signal Transduct Target Ther. 2020;5(1):87.
- Li B, Yang L, Peng X, et al. Emerging mechanisms and applications of ferroptosis in the treatment of resistant cancers [J]. Biomed Pharmacother. 2020:130:110710.
- Lu Y, Chan YT, Tan HY, et al. Epigenetic regulation of ferroptosis via ETS1/miR-23a-3p/ACSL4 axis mediates sorafenib resistance in human hepatocellular carcinoma [J]. J Exp Clin Cancer Res. 2022;41(1):3.
- Shi Z, Li Z, Jin B, et al. Loss of LncRNA DUXAP8 synergistically enhanced sorafenib induced ferroptosis in hepatocellular carcinoma via SLC7A11 depalmitoylation [J]. Clin Transl Med. 2023;13(6):e1300.
- Gao Y, Tong M, Wong TL, et al. Long noncoding RNA URB1-Antisense RNA 1
 (AS1) suppresses Sorafenib-Induced ferroptosis in Hepatocellular Carcinoma by driving Ferritin Phase separation [J]. ACS Nano. 2023;17(22):22240–58.
- 26. Wang Y, Wu X, Ren Z, et al. Overcoming cancer chemotherapy resistance by the induction of ferroptosis [J]. Drug Resist Updat. 2023;66:100916.
- Wang Z, Zong H, Liu W, et al. Augmented ERO1α upon mTORC1 activation induces ferroptosis resistance and tumor progression via upregulation of SLC7A11 [J]. J Exp Clin Cancer Res. 2024;43(1):112.
- Luo Y, Xiang W, Liu Z, et al. Functional role of the SLC7A11-AS1/xCT axis in the development of gastric cancer cisplatin-resistance by a GSH-dependent mechanism [J]. Free Radic Biol Med. 2022;184:53–65.
- Sanger HL, Klotz G, Riesner D, et al. Viroids are single-stranded covalently closed circular RNA molecules existing as highly base-paired rod-like structures [J]. Proc Natl Acad Sci U S A. 1976;73(11):3852–6.

- 30. Zhou WY, Cai ZR, Liu J, et al. Circular RNA: metabolism, functions and interactions with proteins [J]. Mol Cancer. 2020;19(1):172.
- Jeck WR, Sharpless NE. Detecting and characterizing circular RNAs [J]. Nat Biotechnol. 2014;32(5):453–61.
- 32. Wang C, Liu WR, Tan S, et al. Characterization of distinct circular RNA signatures in solid tumors [J]. Mol Cancer. 2022;21(1):63.
- Kristensen LS, Jakobsen T, Hager H, et al. The emerging roles of circRNAs in cancer and oncology [J]. Nat Rev Clin Oncol. 2022;19(3):188–206.
- Wang C, Zhang M, Liu Y, et al. CircRNF10 triggers a positive feedback loop to facilitate progression of glioblastoma via redeploying the ferroptosis defense in GSCs [J]. J Exp Clin Cancer Res. 2023;42(1):242.
- Chai B, Wu Y, Yang H, et al. Tau aggregation-dependent lipid peroxide Accumulation Driven by the hsa_circ_0001546/14-3-3/CAMK2D/Tau complex inhibits epithelial ovarian Cancer peritoneal metastasis [J]. Adv Sci (Weinh). 2024;11(23):e2310134.
- 36. Xu X, Zhang J, Tian Y, et al. CircRNA inhibits DNA damage repair by interacting with host gene [J]. Mol Cancer. 2020;19(1):128.
- Chen R, Yang T, Jin B, et al. CircTmeff1 promotes muscle atrophy by interacting with TDP-43 and Encoding A Novel TMEFF1-339aa protein [J]. Adv Sci (Weinh). 2023;10(17):e2206732.
- Tang Q, Wen H, Hu H, et al. Circ_0070203 promotes epithelial-mesenchymal transition in ovarian serous cystadenocarcinoma through miR-370-3p/ TGFβR2 Axis [J]. Recent Pat Anticancer Drug Discov. 2024;19(2):233–46.
- Zhou X, Zhan L, Huang K, et al. The functions and clinical significance of circRNAs in hematological malignancies [J]. J Hematol Oncol. 2020;13(1):138.
- Wu Y, Xu M, Feng Z, et al. AUF1-induced circular RNA hsa_circ_0010467 promotes platinum resistance of ovarian cancer through miR-637/LIF/STAT3 axis [J]. Cell Mol Life Sci. 2023;80(9):256.
- Zhou X, Liu K, Cui J, et al. Circ-MBOAT2 knockdown represses tumor progression and glutamine catabolism by miR-433-3p/GOT1 axis in pancreatic cancer [J]. J Exp Clin Cancer Res. 2021;40(1):124.
- 42. Dong LF, Chen FF, Fan YF et al. circ-0000512 inhibits PD-L1 ubiquitination through sponging miR-622/CMTM6 axis to promote triple-negative breast cancer and immune escape [J]. J Immunother Cancer, 2023, 11(6).
- 43. Lei M, Zheng G, Ning Q, et al. Translation and functional roles of circular RNAs in human cancer [J]. Mol Cancer. 2020;19(1):30.
- Koppula P, Zhang Y, Zhuang L, et al. Amino acid transporter SLC7A11/xCT at the crossroads of regulating redox homeostasis and nutrient dependency of cancer [J]. Cancer Commun (Lond). 2018;38(1):12.
- 45. Liu T, Jiang L, Tavana O, et al. The deubiquitylase OTUB1 mediates ferroptosis via stabilization of SLC7A11 [J]. Cancer Res. 2019;79(8):1913–24.
- Ruiu R, Cossu C, Iacoviello A, et al. Cystine/glutamate antiporter xCT deficiency reduces metastasis without impairing immune system function in breast cancer mouse models [J]. J Exp Clin Cancer Res. 2023;42(1):254.
- Zheng H, Liu J, Cheng Q, et al. Targeted activation of ferroptosis in colorectal cancer via LGR4 targeting overcomes acquired drug resistance [J]. Nat Cancer. 2024;5(4):572–89.
- Tang B, Zhu J, Wang Y, et al. Targeted xCT-mediated ferroptosis and Protumoral polarization of Macrophages is effective against HCC and enhances the efficacy of the Anti-PD-1/L1 response [J]. Adv Sci (Weinh). 2023;10(2):e2203973.
- Lang X, Green MD, Wang W, et al. Radiotherapy and Immunotherapy Promote Tumoral lipid oxidation and ferroptosis via synergistic repression of SLC7A11 [J]. Cancer Discov. 2019;9(12):1673–85.

Publisher's note

Springer Nature remains neutral with regard to jurisdictional claims in published maps and institutional affiliations.